Department of Precision and Microsystems Engineering

An interface-enriched finite element method for immersed contact under large deformation kinematics

Davis Pazars

Report no : 2022.004
Coach : Alejandro Aragón, Jovana Jovanova, Mary Frecker
Professor : Alejandro Aragón, Jovana Jovanova, Mary Frecker
Specialisation : Engineering Mechanics
Type of report : Master's thesis
Date : 20 January 2022

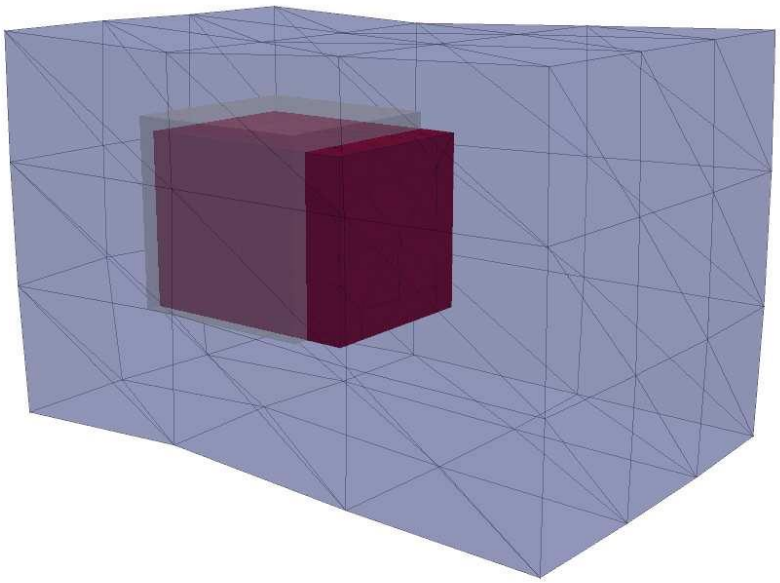

TU Delft Delft University of Technology

Challenge the future

AN INTERFACE-ENRICHED FINITE ELEMENT METHOD FOR IMMERSED CONTACT UNDER LARGE DEFORMATION KINEMATICS

DEPARTMENT OF PRECISION AND MICROSYSTEMS ENGINEERING

by

Davis PAZARS

in partial fulfillment of the requirements for the degree of

Master of Science
in Mechanical Engineering

at the Delft University of Technology,
to be defended publicly on January 28th, 2022.

Student number:	4615727
Project duration:	September, 2020 - January, 2022
Project supervisors:	Dr. A.M. Aragón, TU Delft
	Dr. J. Jovanova, TU Delft
	Prof. M. Frecker, Penn State University
Thesis committee:	Dr. A.M. Aragón, TU Delft
	Dr. J. Jovanova, TU Delft
	Prof. M. Frecker, Penn State University
	Dr.ir. M. Langelaar, TU Delft

TU Delft Delft University of Technology

CONTENTS

1

INTRODUCTION

Although various numerical analysis and optimization tools such as those based on finite element methods have been developed for decades, there are still plethora of challenging applications that require to push the state-of-the-art further. One such application is the design synthesis of compliant mechanisms (CMs), which in essence are mechanisms that deform during actuation. Such mechanisms can be designed monolithic, providing various advantages over traditional mechanisms, such as reduced wear and backlash, as well as no lubrication and assembly. Two interesting subcategories of CMs are contact-aided compliant mechanisms (CCMs) and cellular arrays of contact-aided compliant mechanisms (C3Ms). Initially introduced by Mankame and Ananthasuresh as a way to design CMs that follow a non-linear, non-smooth actuation path [1], these mechanisms experience internal or external contact during actuation. The difference between CCMs and C3Ms is that the latter is a pattern of a unit cell, where an isolated unit cell can be regarded as a CCM. The distinction between the two is made because patterning a unit cell designed to meet specific properties is common practice in the field of metamaterial design. Example applications of CCMs include high precision safety and arming devices [2], ornithopters [3], and surgical instruments [4, 5, 6]. Potential applications for C3Ms being investigated are passively morphing aircraft skins [7], and thermal switches for spacecraft [8]. Usually these mechanisms are either based on their rigid counterparts or designed based on experience and intuition, greatly limiting the design potential. Topology optimization could be used to generate novel, unbiased designs but applying it to synthesis of CCMs and C3Ms has proven to be challenging since it requires a general optimization framework that can accurately analyse 3D structures in contact and under large deformations.

The first reported work on CCM or C3M topology optimization was published by Mankame and Ananthasuresh [9]. The objective was to trace non-smooth paths and the objective function was defined as the distance error between a set of points along the desired and achieved paths. The optimization procedure either removed or inserted frame elements at predefined locations and orientations. Frictionless, adhesionless contact with an external rigid body was assumed. The model considered only small deformations and a linear elastic material model in 2D. The same authors later extended

the model to support large deformations and redefined the objective function in terms of Fourier shape descriptors (FSDs) [10]. Mehta *et al.*[11] optimized unit cells to maximise global strain in a two step procedure. First, an inverse homogenization optimization problem was defined and solved using SIMP for a continuum 2D cell. After that, the cell was converted to a frame structure with a certain number of points along it. A simple contact mechanism resembling a dashpot was inserted to connect any two non-neighboring points, and an exhaustive search was performed to see if any contact mechanism configuration further improves the results of the initial optimization. Nagendra Reddy *et al.*[12] further developed the frame element topology optimization approach presented by Mankame and Ananthasuresh [9, 10]. A contact search algorithm was implemented allowing to model self-contact. The frame elements were allowed to be curved, and also friction was considered. A mutation based stochastic optimization algorithm was used to avoid design sensitivity calculation. The only continuum contact topology optimization model specific to CCMs currently present in the literature was developed by Kumar *et al.*[13]. The objective was to trace a non-smooth path, defined by FSDs. They used circular masks to remove material or add rigid surfaces in the design domain. The position ,as well as the radius of the masks, were set as the design variables of the optimization problem. An active set in conjunction with the Augmented Lagrangian multiplier method were used to enforce contact constraints in a 2D, large deformation setting. A stochastic hill climber search algorithm was then used to advance the design. More recently, the model was extended to handle self-contact [14] and several design optimization examples were presented in [15].

Regarding general (not specific to CCM or C3M design), gradient-based optimization of continuum structures in contact, the main developments can be categorized in density methods such as Solid Isotropic Material with Penalisation (SIMP) or level-set function (LSF) methods [16]. In the context of SIMP-based models, Luo *et al.*[17] first extend the topology optimization to support contact in the geometrically non-linear regime. Contact interfaces were approximated using artificial springs. Jeong *et al.*[18] discretized contact interfaces using the mortar method and optimized the pressure distribution at contact interfaces. Niu *et al.*[19] presented an elastic-elastic body contact optimization method, but assumed that contact surfaces do no change shape. In a later paper [20], the same authors developed a set of rules for a more efficient adjoint sensitivity analysis. Kristiansen *et al.*[21] developed an optimization objective allowing to minimize contact pressure variance for an unknown contact surface area of a deformable body in contact with a rigid surface. Bluhm *et al.*[22] showed that the void elements often used to define the optimization domain can be used to model contact without explicitly enforcing any contact constraints. A detailed comparison of the LSF method implemented in XFEM (LSF-XFEM) and the SIMP method was done by Villanueva and Maute [23]. They concluded that LSF-XFEM can resolve crisp boundaries and accurate contact pressures with coarser meshes compared to SIMP. They also point out that unlike SIMP, LSF-XFEM lacks feature size control and is considerably more difficult to extend to 3D. Lawry and Maute [24] then used LSF-XFEM to optimize 2D elastic-elastic body contact in the small deformation regime and found that XFEM causes convergence issues due to stress oscillations near small intersections. Stability was improved by the same authors using a so-called ghost penalty method [25]. Fernandez *et al.*[26] presented an optimization strategy al-

lowing to optimize multiple contacting 3D deformable bodies in the large deformation regime. The geometry is represented exactly using B-splines and the contact pressures are resolved using the Augmented Lagrangian and mortar methods. So far none of the mentioned frameworks can be used in a truly general large deformation, contact topology optimization setting in 3D. Although [26] comes close, its major disadvantages are the limitations of XFEM such as non-trivial application of Dirichlet boundary conditions or solution accuracy in blending elements. Most of these issues are addressed in more recent enriched finite element methods such as the Interface-enriched Generalized Finite Element Method (IGFEM) [27], providing a better backbone for a truly general contact topology optimization framework.

Inspired by the potential applications of CCMs/C3Ms and informed about the shortcomings of current state-of-the-art frameworks, this research aims to pave the way towards the synthesis of novel CCMs/C3Ms using topology optimization using IGFEM. So far, a novel topology optimization method has been developed by van den Boom *et al.*[28], in which Radial Basis Functions (RBFs) are used to construct the level set function in addition to an elegant contact discretization strategy developed by Liu *et al.*[1] that places enriched nodes at regions of contact to establish a Node-to-Node (NTN) formulation, overcoming the limitations of early NTN and Surface-to-Surface (STS) methods, complexity of Mortar methods, as well as stress oscillations reported in [24].

However, before general contact topology optimization can be accomplished, several smaller objectives still need to be pursued. The specific objectives of this paper is to incorporate and verify large deformation theory in the current IGFEM formulation. Additionally, it aims to clearly illustrate common issues of large deformation and contact problems when the structure of interest is immersed in a void domain, as is commonplace in topology optimization, and develop a strategy to bypass these issues.

The sections of the paper are organized as follows. The first chapter introduces the reader to the relevant existing research and motivates the goal of this project 2.1. Then the problem mechanics and all relevant parameters are defined 2.2. The proposed method for dealing with void element instability is given in 2.3 and several examples are explored in 2.4. Concluding remarks follow in 2.5 and a personal reflection of the project is written in 3.

[1] Article currently under review

2

AN INTERFACE-ENRICHED FINITE ELEMENT METHOD FOR IMMERSED CONTACT UNDER LARGE DEFORMATION KINEMATICS

2.1. INTRODUCTION

Studying and optimizing structures that experience self or external contact while also deforming significantly is necessary in various engineering disciplines. For example, such studies can help improve manufacturing processes in metallurgy, improve the safety of vehicles by means of crashworthiness analysis in the automotive industry, or even improve surgical instruments [6]. However, contact introduces several challenges that scientists have been trying to solve for decades.

In contact problems it is required to enforce additional kinematic constraints between contacting surfaces to guarantee impenetrability and accurate pressure estimates. Calculating constraint conditions for all possible node pairs would be extremely inefficient, so it is common to either specify the contacting surfaces *a priori* or develop an algorithm to automatically detect contacting points/surfaces. The later approach is more challenging, but also a necessity in certain scenarios such as topology optimization or remeshing. Another challenging aspect of solving contact problems is system stability. Due to the highly nonlinear, non-smooth system behaviour, caused by the abrupt changes between states of contact and no contact, the solution algorithm can easily fail. This was especially true for early kinematic constraint enforcement strategies based solely on penalty terms in the stiffness matrix or the introduction of Lagrange multipliers.

The penalty method continuously increases the stiffness of nodes as the gap between them decreases. It is only an approximate enforcement of contact kinematics and can lead to surface penetration if the penalty parameter is too low. Conversely, if the penalty parameter is too high, the system of equations becomes ill-conditioned. In the Lagrange multiplier method, the multipliers are added to the system as additional unknowns and physically can be interpreted as the contact force. These methods are the foundations for more advanced approaches, and the interested reader is advised to study Chapter 1

of Wriggers's textbook [29] for a more thorough explanation. Because the Lagrange multiplier is a force while structural contact problems typically solve for displacement, the final formulation consists of mixed type of variables Mixed formulations (also called hybrid), need to satisfy the *inf-sup* condition, also known as the Ladyzhenskaya-Babuška-Brezzi (LBB) condition [30]. In practice, verifying this condition is not trivial and analytical proofs are rare. The most widely used method to enforce contact constraints in current literature is a hybrid procedure called the augmented Lagrange multiplier method. Here, Lagrange multipliers representing the contact force are added to the system as unknowns and a smoothing penalty term is added to the stiffness matrix for stability. The penalty and multipliers are related by a mathematical expression such that accurate tractions can always be recovered. To avoid increasing the size of the system, research is also being done on Nitsche methods, or simply stable penalty methods [31, 32, 33]. In these methods the continuity of the solution is enforced weakly by considering the stress in each body and adding an additional penalty term, hence the derivation of these methods is confined to a specific constitutive model and cannot be applied in a general setting.

Besides enforcing kinematic constraints, another challenge is discretization of the contact problem. Various methods have been developed over the years for the standard formulation of FEM such as Node-to-Node (NTN) [34], Node-to-Surface (NTS) [35], or Surface-to-Surface (STS) [36], however all of them suffer from additional issues. NTN is narrowly confined to problems with conforming contact meshes. Meaning, if an element node along one of the contacting surfaces does not overlap with a node on the other surface, the displacement field becomes discontinuous. However, in a general setting it is not realistic to expect meshes where nodes at contacting surfaces perfectly overlap. Besides that, NTN is also only applicable for problems with small deformations and no sliding. Single pass (one master and one slave surface) NTS fails to pass the contact patch test while a dual pass (both surfaces are master and slave) leads to locking due to overconstraining. STS surpasses the limitations of NTN and NTS, but might not always work well in practice because many difficult exception cases need to be considered, see 8.4.1 in [29]. Another family of methods are the Mortar methods, in which the nodes of both surfaces are projected in to a fictitious intermediate surface. Across this surface contact kinematics are enforced using the augmented Lagrange multipliers in a weak sense, integrated, and then the displacement is interpolated back to the original surfaces. The implementation of such methods can be highly complex, especially for 3D problems [37, 38, 26].

A simpler strategy to contact discretization is offered by enriched FEM formulations. These methods enrich the standard FEM formulation with additional functions along discontinuities, which allows to decouple the interfacing surfaces from the mesh. Because contact bears resemblance with a fractured surface in the sense that both lead to a discontinuous displacement field, the majority of the contact problem literature using enriched methods has focused on the eXtended finite element method (XFEM) [39, 40], which was initially developed to solve fracture mechanics problems. It has been shown in [24] that XFEM alone is not sufficient to recover accurate tractions, leading to the development of complex hybrid XFEM-Mortar methods [26, 41] or other stabilization techniques [25, 42]. XFEM also has other fundamental issues such as reduced solution

accuracy in blending elements and the inability to strongly enforce essential (Dirichlet) boundary conditions, and these issues are addressed by other enriched methods such as the interface-enriched generalized finite element method (IGFEM) [27]. A method to solve geometrically linear contact problems in IGFEM has been developed in where enriched nodes are placed at locations that match a node along the other contacting surface, leading to a simple NTN-like discretization approach [1].

Besides convenient discretization of interfaces, there are other benefits of enriched methods. Because standard FEM requires to create geometry conforming meshes, some shapes can be notoriously difficult to mesh efficiently and can lead to ill-shaped elements, which degrade the accuracy of the final result. Using enriched methods such as IGFEM, it becomes possible to immerse complex geometries in a simple background structured mesh [43]. Besides simplifying meshing, immersion of geometry within some domain is also typical for level set based topology optimization methods. When a geometry is immersed, the surrounding material is typically assigned a void material. The void is assigned minuscule stiffness such that it has as little of an influence on the final solution as possible, but also does not lead to an ill-conditioned stiffness matrix. This approach works well in the small deformation regime but can lead to instabilities in an iterative solution procedure or non-physical behaviour due to deformation-induced stiffness in the void elements [22]. Various approaches have been proposed to deal with this problem. Buhl, Pedersen, and Sigmund [44, 45] relaxed the solution convergence criterion by removing degrees of freedom next to void elements from the error estimate. Klarbring *et al.* [46] used common hyperelastic constitutive laws to model the void while Lahuerta *et al.* [47] investigated the use of polyconvex materials. Yoon *et al.* [48] kept the entire domain solid by the introduction of zero-length elements with stiffness and inter-element connectivity information. These additional elements can disappear during optimization by means of penalization. Wang *et al.* [49] reduced the analysis of void elements from non-linear to liner to avoid displacement-induced effects. Bruns *et al.* [50] developed a void element removal and reintroduction strategy. Behrou *et al.* [51] built upon [50] to achieve better computational performance by using a more sophisticated density filter. They also mention that, after testing all the other mentioned methods, none provided satisfactory results in all of their test cases. So far, all of these methods have been developed for standard FEM in the context of density-based topology optimization.

So far it was discussed that IGFEM has the potential to more accurately solve contact problems compared to XFEM and that it can be used to immerse geometry for complex meshing scenarios or topology optimization. The primary goal of this project is to combine the works of [1] and [43] and extend the capabilities to solve large deformation, immersed contact problems. In anticipation of the mentioned void element issues in the large deformation regime, this project also aims to develop a method for void element removal and reintroduction in IGFEM. Besides the obvious ability to solve geometrically non-linear, immersed contact problems, the proposed work would also pave way for geometrically non-linear contact topology optimization in IGFEM.

[1] Article currently under review

2.2. PROBLEM DESCRIPTION AND FORMULATION

Consider a domain Ω in d-dimensional Euclidian space, i.e., $\Omega \subset \mathbb{R}^d$ (for convenience, Ω is displayed as a 2D domain in Figure 2.1). It consists of two deformable bodies in their undeformed Ω_i and deformed ω_i states. The undeformed state is called the initial or reference configuration while the deformed state can be referred to as the current configuration. In this work, a total Lagrangian formulation is used, meaning the initial configuration is used as the basis for equilibrium and constitutive relations.

The body Ω_i boundaries are given by $\partial\Omega_i \equiv \Gamma_i$ and their normals by $\mathbb{N}_i$. Following the body notation, lowercase letters are used to describe the boundaries and their normals in the deformed configuration. These boundaries consist of several disjoint regions $\Gamma_i^u \cap \Gamma_i^t = \emptyset$ attributed to different types of boundary conditions $\Gamma_i = \Gamma_i^u \cup \Gamma_i^t \cup \Gamma_i^g \cup \Gamma_i^c$. Dirichlet (essential) and Neumann (natural) boundary conditions are denoted by Γ^u and Γ^t while interface and contact boundaries by Γ^g and Γ^c respectively. Potential contact surfaces, shown by dashed lines in Figure 2.1, are usually identified *a priori* for computational efficiency.

The motion of a body is described by the mapping $\boldsymbol{\phi} : \Omega \to \omega \subset R^d$. Across this motion, each particle in the body $\boldsymbol{X} \in \Omega$ is displaced to $\boldsymbol{x} = \boldsymbol{\phi}(\boldsymbol{X}) = \boldsymbol{X} + \boldsymbol{u}(\boldsymbol{X})$, with $\boldsymbol{u}$ denoting the displacement.

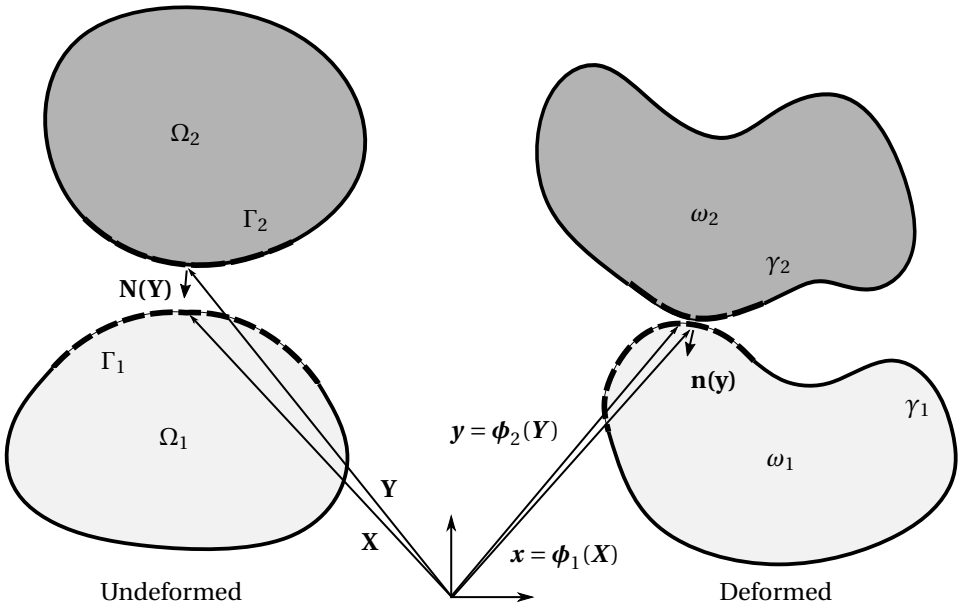

Figure 2.1: Problem schematic showing two bodies that come into contact in their deformed states. Capital letters are used for the undeformed state, lowercase letters for the deformed. Subscript indices are used to number the bodies.

Given a body force $\boldsymbol{b}_i : \Omega_i \to \mathbb{R}^d$, prescribed displacement $\bar{\boldsymbol{u}} : \Gamma_i^u \to \mathbb{R}^d$, and traction $\bar{\boldsymbol{t}} : \Gamma_i^t \to \mathbb{R}^d$, the goal is to find the displacement field $\boldsymbol{u}$ from the elastostatics equilibrium equation, expressed in strong form as

$$\nabla \cdot (\boldsymbol{F}_i \boldsymbol{S}_i) + \boldsymbol{b_i} = \boldsymbol{0} \qquad \text{in } \Omega_i, \tag{2.1}$$

while subjected to boundary conditions

$$\boldsymbol{u_i} = \bar{\boldsymbol{u}}_i \qquad \text{on } \Gamma_i^u, \tag{2.2}$$

$$(\boldsymbol{F_i S_i})\boldsymbol{n}_i = \bar{\boldsymbol{t}}_i \qquad \text{on } \Gamma_i^t, \tag{2.3}$$

and contact conditions

$$p_n = \boldsymbol{t}_1^c \cdot \boldsymbol{n}_1 \leq 0 \qquad \text{on } \gamma^c, \tag{2.4}$$

$$g_n = (\boldsymbol{x}_2 - \boldsymbol{x}_1) \cdot \boldsymbol{n}_1 \geq 0 \qquad \text{on } \gamma^c, \tag{2.5}$$

$$p_n g_n = 0 \qquad \text{on } \gamma^c. \tag{2.6}$$

In these equations, $\boldsymbol{F} = \nabla \boldsymbol{\phi} = \boldsymbol{I} + \nabla \boldsymbol{u}$ is the deformation gradient, $\boldsymbol{S}$ is the second Piola-Kirchhoff stress tensoris $\boldsymbol{S}$, and the product of the two is the well-known Cauchy stress tensor $\boldsymbol{\sigma} = \boldsymbol{FS}$. A nearly incompressible Mooney-Rivlin material formulation with a strain energy density function $W(J_1, J_2, J_3) = C_{10}(J_1 - 3) + C_{01}(J_2 - 3) + D_1(J_3 - 1)^2$ was used to describe solid material, while in some cases in an emmersed setting a basic St. Venant-Kirchhoff formulation $W(\mathbf{E}) = \frac{\lambda}{2}[\text{tr}(\mathbf{E})]^2 + \mu \text{tr}(\mathbf{E}^2)$ was used for void material. Details of these constitutive laws are provided in Appendix A. Displacements and tractions are transferred across the perfectly bonded interfaces Γ_{ij}^g while contact kinematics are enforced by the Hertz-Signorini-Moreau conditions, also referred to as Karush-Kuhn-Tucker conditions [29]. These conditions state that the contact pressure p_n can only be compressive (2.4), that contacting bodies cannot penetrate each other (2.5), and that there is no contact pressure if there is a contact gap (2.6).

The weak form of the governing equations can be expressed as a minimization problem of the functional

$$\boldsymbol{\Phi}(\boldsymbol{u}, \boldsymbol{\lambda}^g, \boldsymbol{\lambda}^c) = \sum_{i=1}^{3} \Pi_i(\boldsymbol{u}_i) + \Pi_c(\boldsymbol{u}_1, \boldsymbol{u}_2, \boldsymbol{\lambda}^c), \tag{2.7}$$

in which Π_i is the strain energy of the deformable bodies, while Π^g and Π^c are terms associated with interface and contact constraints:

$$\Pi_i(\boldsymbol{u}_i) = \int_{\Omega_i} \nabla \boldsymbol{w} \cdot \boldsymbol{S} dV - \int_{\Omega_i} \boldsymbol{w} \cdot \boldsymbol{b} dV - \int_{\Gamma_i^t} \bar{\boldsymbol{t}} \cdot \boldsymbol{w} dA = 0, \tag{2.8}$$

$$\Pi_c\left(\boldsymbol{u}_1, \boldsymbol{u}_2, \boldsymbol{\lambda}^c\right) = \int_{\Gamma^c} \frac{1}{2\epsilon_n} \left[\langle \hat{\lambda}_n \rangle^2 - \lambda_c^2 \right] d\Gamma. \tag{2.9}$$

A standard method using Lagrange multipliers $\boldsymbol{\lambda}^g$ is used to enforce the interface conditions and an augmented Lagrange multiplier method using $\boldsymbol{\lambda}^c$ as the multipliers is implemented to enforce the contact conditions, because for contact problems the standard method is prone to stability issues. The augmented multiplier is defined as $\hat{\lambda}_n = \lambda_n + \epsilon_n g_n$, where ϵ_n is the penalty parameter and $\lambda_n = \lambda^c \cdot \boldsymbol{n}$ is the Lagrange multiplier normal component. Lastly, $< \bullet >$ is the Macaulay bracket notation.

If a domain $\Delta \subset R^d$ is defined that fully encloses the original domain $\Delta \supseteq \Omega$ and discretized $\Delta^h = \cup_i e_i$ into non-overlapping finite elements $e_i \cap e_j = \emptyset, \forall i \neq j$, then the discretized weak form of the governing equations can be solved by choosing a trial solution and weight function from the interface-enriched finite element space

$$\mathscr{S}_e = \{\boldsymbol{u}^h \big| \boldsymbol{u}^h(\boldsymbol{x}) = \underbrace{\sum_{i \in \iota_h} N_i(\boldsymbol{x})\boldsymbol{u}_i}_{\text{std. FEM}} + \underbrace{\sum_{i \in \iota_e} s_i \phi_i(\boldsymbol{x})\boldsymbol{\alpha}_i}_{\text{enrichment}}, \quad \boldsymbol{u}_i, \boldsymbol{\alpha}_i \in \mathbb{R}^d\}. \tag{2.10}$$

Here the solution consists of two contributions. One is from the standard FEM with ι_h being the index set of all standard nodes and N_i the ith Lagrange shape function associated with degrees of freedom $\boldsymbol{u}_i$. The second contribution comes from the enrichments, where similarly ι_e denotes the index set of all enriched nodes and ψ_i is the enrichment function associated with the enriched degrees of freedom $\boldsymbol{\alpha}_i$. A scaling factor s_i is added to improve the condition number of the system matrix. As shown in Figure 2.2, enriched nodes are created at contact and material interfaces and intersected elements are divided into integration elements. A hierarchical structure is kept to resolve cases where an element is intersected by multiple interfaces. Further details of the immersed formulation can be found in [43]. A publication on the contact method is currently under review.

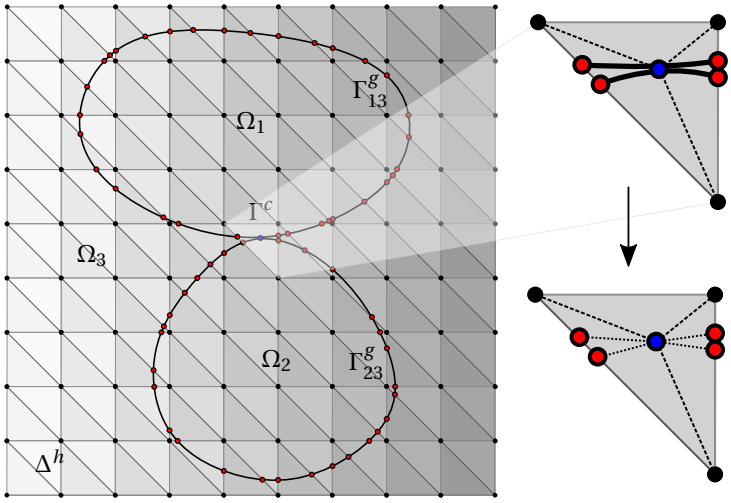

Figure 2.2: Example of locations where enriched nodes are created in an immersed analysis (left) and the creation of integration elements (right). The boundary is discretized in the process and becomes faceted. The blue node represents a contact node while red nodes are interface nodes.

2.3. APPROACH TO VOID ELEMENT INSTABILITY

Immersion can help solve problems where the domain is too complex to create a geometry-conforming mesh. It is also prevalent in topology optimization and fluid-structure interaction problems. For example, in topology optimization it is commonplace to fill the design domain not occupied by the solid structure with void elements. These elements are not needed to solve a system for equilibrium but greatly simplifies updating the topology because the standard degree-of-freedom order in the system is preserved. Ideally, the stiffness of void elements should be zero to not influence the solution, but this would lead to a singular stiffness matrix. Although various methods have been proposed to address void instability [44, 45, 46, 47, 48, 49, 50, 51], only the void element removal techniques by Bruns and Tortorelli [50] and Behrou *et al.* [51] would truly solve the induced stiffness issue. Their method, as well as all the others, is specifically designed for density-based topology optimization and would not work in a simple immersed contact analysis setting. Hence, a simple method for removing and reintroducing void elements within a single analysis step is introduced here.

Given an assembled system $\mathbf{KU} = \mathbf{F}$, where $\mathbf{K}$ is the stiffness matrix, $\mathbf{F}$ the force vector, and $\mathbf{U}$ the displacement vector, an $m \times n, n < m$ transformation matrix $\boldsymbol{T}$ is defined

$$\boldsymbol{T} \coloneqq m \overbrace{\begin{bmatrix} \boldsymbol{I} & \mathbf{0} & . & . & . & \mathbf{0} \\ \mathbf{0} & \boldsymbol{I} & . & . & . & \mathbf{0} \\ . & & . & & & . \\ . & & & . & & . \\ . & & & & . & . \\ \mathbf{0} & \mathbf{0} & . & . & . & \boldsymbol{I} \end{bmatrix}}^{n}, \tag{2.11}$$

and is used to reduce the original system of m degrees of freedom (DOFs) to a system $\tilde{\mathbf{K}}\tilde{\mathbf{U}} = \tilde{\mathbf{F}}$ of n DOFs. The reduced stiffness matrix $\tilde{\mathbf{K}}$ is defined as $\tilde{\mathbf{K}} = \boldsymbol{T}^{\mathsf{T}}\boldsymbol{K}\boldsymbol{T}$ and the reduced force vector as $\tilde{\mathbf{F}} = \boldsymbol{T}^{\mathsf{T}}\boldsymbol{F}$. To assemble $\mathbf{T}$, an $m \times m$ matrix $\mathbf{T}_0$ is initialized. For every DOF $\tilde{m}$ that should be preserved and mapped to $\tilde{n}$, the $\tilde{m} \times \tilde{m}$ entry of $\mathbf{T}_0$ is set to 1. For all other DOFs the value is set to 0. Once done, the empty columns can be removed to arrive at the final $m \times n$ matrix $\mathbf{T}$. Although the reduced system allows to remove any single DOF, in practice removing all DOFs associated with a particular node is required. In other words, if a 2D problem has 2 DOFs for each node, removing just 1 of the 2 would not solve the instability issues for that node. Hence, $\boldsymbol{T}$ can be written in smaller matrices $\mathbf{T_i}$, where each $\mathbf{T_i}$ groups DOFs of node i, and is either an identity matrix or a matrix full of zeros. It is important to note that the DOFs discussed here are only those associated with the standard FEM formulation. The reduced system is solved as usual, and then the original DOF order can be recovered by the transformation $\mathbf{U} = \mathbf{T}\tilde{\mathbf{U}}$. A step-by-step schematic of the full procedure is shown in Figure 2.3.

This method is an alternative void removal and reintroduction for standard large deformation analyses. Since the removal criterion is associated with a material type, not element density, this method is not directly applicable to density-based topology optimizations. Because all void elements are removed, this method also supports contact

analyses. As will be shown in a later example, void elements can alter contact kinematics, so stability in the large deformation setting alone is not enough for accurate results in large deformation contact problems. Additionally, the void elements are both removed and reintroduced in the analysis step, whereas in [51] the optimization step is performed on the reduced system and DOFs are reintroduced based on sensitivity analysis results.

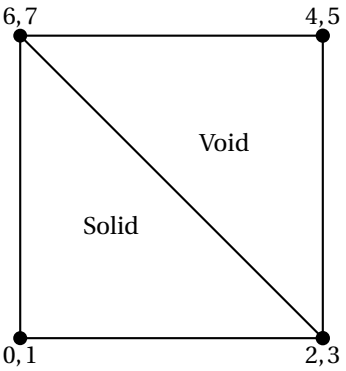

$$\begin{array}{c} \\ 0 \\ 1 \\ 2 \\ 3 \\ 4 \\ 5 \\ 6 \\ 7 \end{array} \begin{array}{c} \begin{array}{cccccc} 0 & 1 & 2 & 3 & 4 & 5 \end{array} \\ \left[\begin{array}{cc:cc:cc} 1 & 0 & 0 & 0 & 0 & 0 \\ 0 & 1 & 0 & 0 & 0 & 0 \\ \hdashline 0 & 0 & 1 & 0 & 0 & 0 \\ 0 & 0 & 0 & 1 & 0 & 0 \\ \hdashline 0 & 0 & 0 & 0 & 0 & 0 \\ 0 & 0 & 0 & 0 & 0 & 0 \\ \hdashline 0 & 0 & 0 & 0 & 1 & 0 \\ 0 & 0 & 0 & 0 & 0 & 1 \end{array}\right] \end{array}$$

Figure 2.3: A simple system with 1 solid and 1 void element, where each node has 2 DOFs (left figure). The DOF numbers are shown at each node. Assembled transformation matrix $\mathbf{T}$ in order to remove the top right node (right figure).

2.4. EXAMPLES

2.4.1. 2D LARGE DEFORMATION BENCHMARK TEST

A 2D C-shaped structure originally published by Yoon and Kim [48] is a popular large deformation example among other researchers [47, 22]. A similar setup is used in this example to verify the large deformation kinematics in 2D.

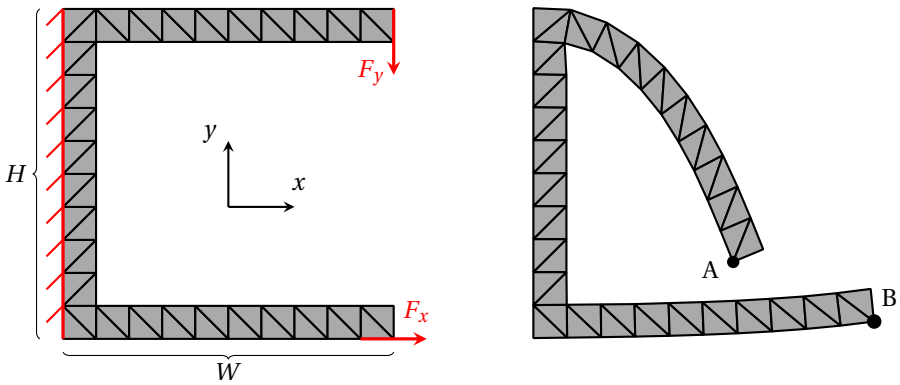

Figure 2.4: C-bar example setup (left) and the deformed shape with marked nodes for which the displacement is verified using commercial finite element analysis software (right)

Here, the 2D C-shaped structure has a height H equal to its width $H = W = 10$. The size of each rectangular partition containing two triangular elements is $H/10$ by $W/10$. The left-most edge is fixed and there are two tractions $F_x = 0.03$ and $F_y = 0.02$ acting on the nodes of a single element's edge. A nearly incompressible Neo-Hookean material model was used with plane strain conditions and constants $C_{10} = 0.1925$, $D_1 = 0.833$ that match linear elastic properties $E = 1$, $\nu = 0.3$ in the small deformation regime. Note that the parameters are given without units for compatibility with any consistent unit system.

Because the inner corners of the structure exhibits a stress singularity, a consistent estimate of the strain energy could not be obtained. Since the mesh used in this example as well as in [48] is coarse, the final displacement varies a lot with even slight mesh modifications. Moreover, the current implementation of the geometric engine uses triangular elements in 2D so it makes sense to verify these, but [48] used rectangular elements, making it even harder to compare results. As an alternative, the results were compared with [48] and commercially available finite element analysis software where the triangular mesh could be replicated exactly. The obtained displacements U^i of nodes $i = \{A, B\}$ in x-direction U_x^i and y-direction U_y^i were

Software	U_x^A	U_y^A	U_x^B	U_y^B
Hybrida (in-house)	-3.95728	-6.69314	0.306307	0.501446
Abaqus (commercial)	-3.95730	-6.69315	0.306307	0.501446

An immersed analysis with and without void removal was also performed. The geometry was kept the same and a simple Neo-Hookean formulation was used for the void with coefficients equivalent to $E = 10^{-12}$ and $\nu = 0$ in linear elasticity. The deformed shapes are shown in Figure 2.5, and in both cases the obtained displacements for control nodes A and B were the same.

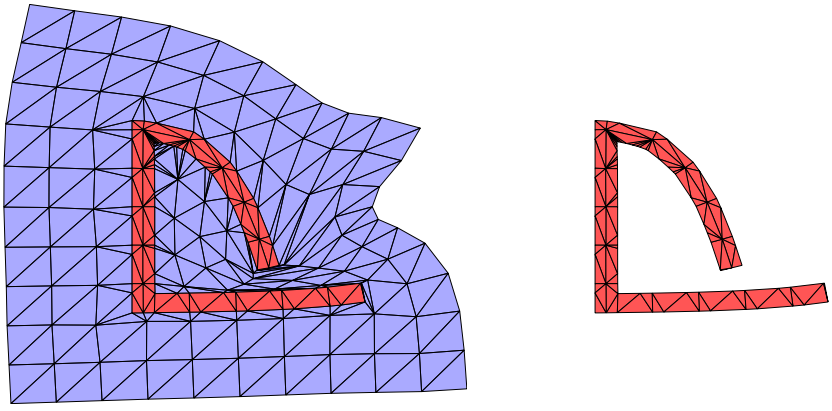

Figure 2.5: Deformed shape of the C-structure in an immersed analysis (left) and the deformed shape for the same problem using the proposed void elimination strategy. The obtained displacement at the control nodes A and B was the same, meaning that for this level of deformation voids do not influence the result significantly.

2.4.2. 3D LARGE DEFORMATION BENCHMARK TEST

A simply supported unit cube shown in Figure 2.6 is subjected to a uniaxial traction load $T_x = 1000$ in the x-direction on face 3. The load is applied in 10 equal increments. Faces 5, 6, and 4 are constrained in x, y, and z-directions respectively. Nearly incompressible Mooney-Rivlin material model was used with coefficients $C_{10} = 80$, $C_{01} = 20$, and $K = 1 \cdot 10^7$ for the solid cube and a St. Venant-Kirchhoff model with Young's modulus $E = 1 \cdot 10^{-6}$ and Poisson's ratio $\nu = 0$ was used for the void elements. The test was performed in both a non-immersed as well as an immersed setting.

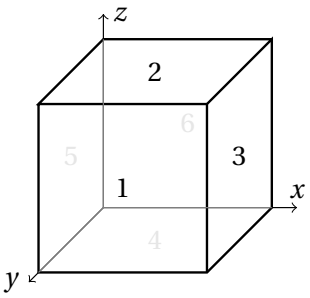

Figure 2.6: 3D unit cube reference.

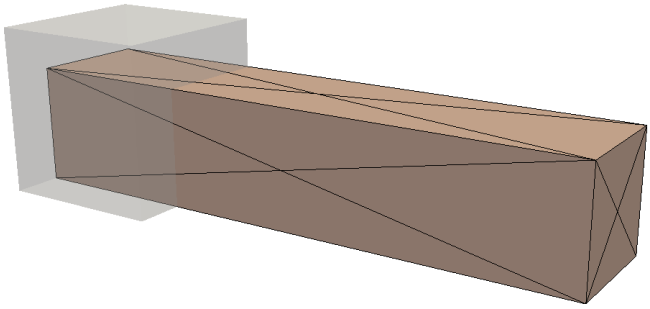

Figure 2.7: Constant Cauchy stress distribution in the deformed 3D unit cube. The deformation was scaled 0.5x. The obtained Cauchy stress value was 6028. The undeformed shape is shown in grey with reduced opacity. The same result is obtained in immersed analysis using the proposed void elimination strategy.

Figure 2.7 shows that an elongation several times the length of the cube yields a constant stress field, as it was expected. The obtained Cauchy stress was 6028, and the same results were obtained in commercially available finite element analysis software. However, the same problem in an immersed setting ran into convergence issues. Figure 2.8 shows that after the first load step, while the deformation is still relatively small, the solution visually seems fine but in the last converged step the void elements have deformed in an obscure way. Even though the stress distribution is still uniform in the solid ele-

ments and zero in the void elements, the solution diverges in the next load step. To try and improve convergence, bigger background meshes were tested to accommodate the deformed cube. In some cases an extra load step converged but never the full analysis, which goes to show that convergence depends on the chosen background mesh. Even if a much larger background mesh would completely converge, there is no guarantee, and for time-costly analyses the extra step of finding a stable background mesh is not a viable option. These issues can be partially alleviated by using more stable material formulations [47], but, as will be shown in the next example, these enhanced materials are not suitable for immersed contact analysis.

Using the proposed void elimination strategy, the same solution was obtained as in the non-immersed analysis, and is shown in Figure 2.7.

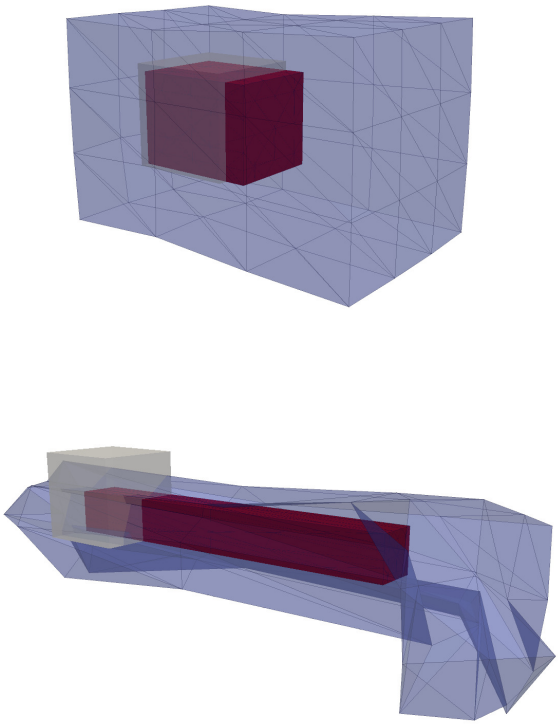

Figure 2.8: Undeformed shape (grey) and deformed shape (red) of the solid cube immersed in background mesh (blue) after 1 load step (top figure) and 7 load steps (bottom figure). A constant stress field is recovered in the solid, and the stress is zero in the void, but the analysis nonetheless diverges in the next load step.

2.4.3. LARGE DEFORMATION CONTACT ANALYSIS

This examples covers non-immersed large deformation contact analysis in 2D and discusses fundamental issues regarding contact in immersed analysis. The C-shaped structure from Section 2.4.1 was slightly modified for this example by extending the top section by 2 units. Also, the horizontal traction F_x was removed. The geometry along with the mesh for the non-immersed case is shown in Figure 2.9 and for the immersed case in Figure 2.10. In the immersed analysis Neo-Hookean material was used for the void elements with constants $C_{10} = 2.5 \cdot 10^{-7}$ and $K = 3.33 \cdot 10^{-7}$, equivalent to a Young's modulus $E = 1 \cdot 10^{-6}$ and Poisson's ratio $\nu = 0$ in linear elasticity. Everything else was kept the same.

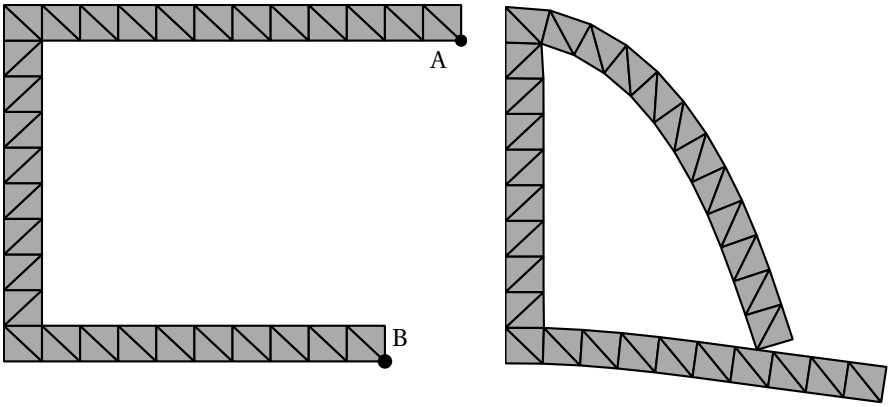

Figure 2.9: Undeformed geometry for the non-immersed large deformation contact analysis with marked control nodes A and B (left). Deformed geometry (right).

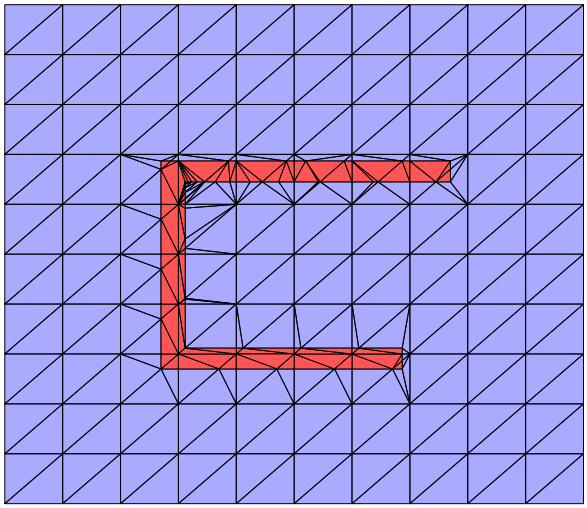

Figure 2.10: Adjusted c-bar structure with an elongated top section for the immersed analysis.

The deformed geometry for the non-immersed large deformation contact analysis is shown in Figure 2.9, and displacement for the control nodes A and B are

Software	U_x^A	U_y^A	U_x^B	U_y^B
Hybrida (in-house)	-5.40459	-8.62097	-0.142732	-1.09039
Abaqus (commercial)	-5.39129	-8.61451	-0.139777	-1.07664

Displacements at these nodes were compared with commercially available finite element analysis software. Reasons for such a comparison method were discussed in detail in Section 2.4.1. The difference in displacement magnitude between the results is only 0.12% for node A and 1.29% for node B. Given that the methods used to discretize the equations of motion are completely different, such a small error margin is fair.

For the immersed analysis the deformed shape is shown in Figure 2.11 and it is clearly visible that the bottom bar has displaced even though no force was applied to it, nor did it come into contact with the top part, and, above all, no kinematic constraints were established in the problem definition. This happens because hyperelastic materials are defined such that the strain energy tends to infinity as the material is compressed. In other words, the more a hyperelastic material is compressed, the stiffer it becomes. Even though void elements are assigned a minuscule stiffness, the deformation-induced stiffness can be so large that these elements start to transfer a load. This is a fundamental issue for immersed contact analyses because there will always be a severely squished void element in-between contacting surfaces, unless the surfaces are already in contact in the undeformed state. In an immersed large deformation setting this stiffening can also be an issue, but in such cases existing methods using enhanced strain energy density formulations could be used to alleviate this problem [47]. Even with a simple hyperelastic material formulation an immersed analysis can converge for relatively large deformations, as was shown in a similar example in Section 2.4.1. This stiffening issue stems from the physical description of a material rather than from the numerical implementation, meaning that as long as there are hyperelastic void elements, this stiffening can be an issue. Non-hyperelastic formulations can be used but these can easily lead to stability issues in the large deformation regime, as was shown in 2.4.2. Bluhm *et al.* [22] used this effect to their advantage as an alternative contact analysis method. Such an approach is called the third medium contact method. Although showing good results, the resulting behaviour of this method is non-physical and it is not clear from their paper if this approach is general or applicable only in certain cases. What is certain though is that the stiffening behaviour is not an issue if no void elements are present in the first place.

Unfortunately, the attempt to extend the immersed large deformation analysis to include contact failed. The unforeseen issues with void elements delayed the project, and the final task of merging the geometric immersion engine and the contact analysis procedures is still ongoing.

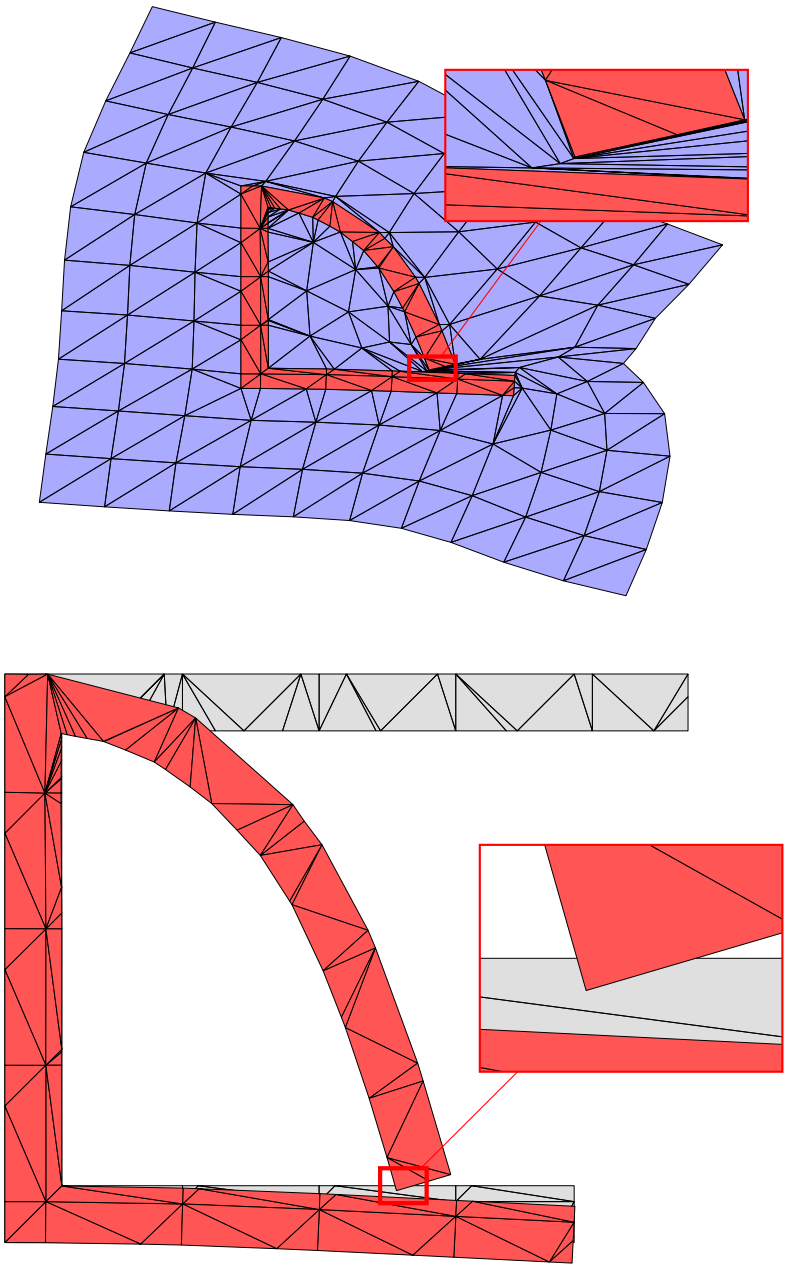

Figure 2.11: Deformed shape of the adjusted C-bar example in an immersed domain with a zoomed-in section of severly compressed elements (top). Deformed shape (red) of the same example with the undeformed shape (grey) in the background and a zoomed-in section showing that the bottom bar has displaced even though no parts of the solid structure are in contact and contact kinematics are not implemented in the analysis (bottom).

2.5. CONCLUSIONS

The purpose of this project was to extend the current capabilities of the finite element analysis library *Hybrida* (developed at TU Delft by A. Aragón and coworkers) to support large deformation contact analysis in an immersed setting.

The set out goal has been achieved partially. Current implementation supports large deformation contact analysis in a non-immersed setting, but only large deformation analysis in an immersed setting. Implementation of the later did not fail, rather the project simply ran out of time before it could be finished. This is in large part due to unforeseen issues with void elements in this type of analysis.

Although void material instabilities were a known issue, the extent to which void materials impact the solution in a contact analysis was unknown to the author. Various enhanced hyperelastic constitutive laws have been formulated to improve void material convergence in the large deformation regime, but contact analysis presents new issues. As any two elements approach contact, the void element in-between is deformed to an extent that the deformation-induced stiffness allows the void element to transfer a load, even though the premise of the void elements is to have as little impact on the final outcome as possible. In other words, the strain energy of the void element tends to infinity, and so does its stiffness. This is a common property for hyperleastic materials, and the only known exception to the author - St. Venant-Kirchhoff material - is known to be unstable (also shown in this study).

To solve this issue, an additional literature study was performed to investigate existing options to deal with these void elements. It was decided to develop a method to eliminate the voids for the analysis part and afterwards reintroduce them without losing the original node order defined in the beginning. The preservation of node order would be useful in topology optimization, if such a research direction is pursued in the future.

The final task left to finish the set out goal is to merge the geometric engine responsible for immersion with the contact analysis procedures. Initial work on this topic has already begun, but initial time estimates proved to underestimate the extent of the task and the current issue with the merging is not fully understood. After that, only minor adjustments are expected to extend the merged solution to support large deformation kinematics, as that was also the case for non-immersed analysis.

3

REFLECTION

Initially, the goal of the project was centered around topology optimization of self contacting compliant mechanisms. The most important required components such as the topology optimization framework or the contact analysis procedure had already been implemented, and it was expected that only large deformation analysis was missing before work on topology optimization could begin. As such, the literature study focused mostly on topology optimization and the methodologies of solving the physical problem were only broadly studied for a general overview. After all, the contact analysis was already in place and large deformation kinematics is a solved problem. However, as support for large deformation kinematics was finished, a previously unexpected issue with void elements arose that later became the center point of the project. The complex relationship between material and geometrical non-linearities was underestimated and, frankly, almost completely unreported in the work studied during the literature study. Only one study on large deformation contact topology optimization addressed this issue, and this study was made public only during this project.

Amidst the initial excitement and ambition, it is easy to become too reliant on a smooth road towards success, so this project served as a good lesson to always plan for contingencies and expect that there will be issues that one does not know about at the time of making the plan. Also, even though I initially perceived the change of plans as a failure of the initial goal, in the big picture it is actually quite exciting to see that there are still many interesting challenges to solve in a decades-old field, and the the end result has so much potential. Even if just one researcher finds this work insightful and it helps them better identify future research topics, I would consider this project as a success.

Beyond the theory and literature, this project required learning multiple other valuable skills that will likely benefit in the future like dealing with version control tools, efficiently debugging the code, or writing robust unit tests. It is also the experience of being immersed in a programming project of a completely different scale compared to course assignments and homework that has immense value. From personal experience, the coursework programming assignments are mostly focused on getting some desired result. How efficiently this is achieved rarely matters and these codes rarely span more than a few hundred lines of code. When starting this project, I was suddenly faced with

a library spanning several tens of thousands lines of code, with a steep learning curve and little documentation. The problem at hand no longer required just any solution, but a scalable solution that fits well into the existing code architecture. Although there were times where the lack of instructions how to operate within this code was frustrating, overall I enjoyed tinkering around and trying to understand why things are being done the way they are.

Lastly, even though the initial objective was not achieved, I cannot say the same about my personal goals. My first hands-on experience with finite element analysis (FEA) was at a student rocketry team Delft Aerospace Rocket Engineering (DARE) during Bachelor's studies. Here I worked on predicting the failure load of a thin-walled composite shell structure. I was eager to learn more in-depth about how these complex programs work under the hood, and this experience inspired the choice of my Master's degree specialization. Having completed several courses on numerical methods and advanced mechanics, as well as having contributed during this project to a state-of-the-art FEA library to solve problems that were few people can solve, I can proudly say that I have surpassed my expectations for this degree program and that I am looking forward to applying this knowledge to solving important real-world problems.

A

CONSTITUTIVE MODELS

A nearly incompressible neo-Hookean and a St. Venant-Kirchhoff material laws were used throughout this work. The neo-Hookean model was derived from a nearly incompressible Mooney-Rivlin material model, described by the strain energy density function

$$W(J_1, J_2, J_3) = C_{10}(J_1 - 3) + C_{01}(J_2 - 3) + D_1(J_3 - 1)^2, \tag{A.1}$$

which is defined in terms of the reduced invariants $J_1 = I_1 I_3^{-1/3}$, $J_2 = I_2 I_3^{-2/3}$, $J_3 = I_3^{1/2}$, where I_1, I_2, I_3 are the invariants of the right Cauchy-Green tensor $\mathbf{C}$. The reduced invariants separate the dilatation (volume change) and distortion parts of the strain energy. Since nearly incompressible hyperelastic materials are stiff in dilatation (volume change) but compliant in distortion, it is necessary to separate energies of these deformation modes because the large difference in stiffness can otherwise cause numerical instability [52]. The C_{10} and C_{01} terms in W are material coefficients and D_1 is the penalty term imposing near incompressibility. All 3 terms are set by the user.

In the special case when $C_{01} = 0$, this model reduces to the nearly incompressible neo-Hookean model and is a more convenient choice because it has a simple connection to linear elasticity – in the small deformation regime the constant $C_{10} = \mu/2$ relates to the shear modulus μ, and $D_1 = K/2$ to the bulk modulus K.

The 2$^{\text{nd}}$ Piola-Kirchhoff stress $\boldsymbol{S} = C_{10}\boldsymbol{J}_{1,\boldsymbol{E}} + C_{01}\boldsymbol{J}_{2,\boldsymbol{E}} + 2D_1(\boldsymbol{J}_3 - 1)\boldsymbol{J}_{3,\boldsymbol{E}}$ is obtained by differentiating the strain energy density function W with respect to the Green-Lagrange strain $\boldsymbol{E} = 1/2(\boldsymbol{C} - \boldsymbol{I})$, where $\mathbf{J}_{i,\mathbf{E}}$ is the vector of all derivatives of J_i with respect to $\mathbf{E}$. The constitutive tensor $\mathscr{C}$ is obtained by differentiating W twice with respect to $\boldsymbol{E}$.

Besides the neo-Hookean model, in some examples the St. Venant-Kirchhoff material model was used for void elements. This model is an extension of linear elasticity and defines a linear stress-strain relationship between the energetically conjugate $\boldsymbol{E}$ and $\mathbf{S}$. Its strain energy density is given by

$$W(\mathbf{E}) = \frac{\lambda}{2}[\mathrm{tr}(\mathbf{E})]^2 + \mu \mathrm{tr}(\mathbf{E}^2), \tag{A.2}$$

where λ is Lamé's first parameter. The procedure for obtaining the stress vector and constitutive matrix is the same as before.

BIBLIOGRAPHY

[1] Nilesh D Mankame and GK Ananthasuresh. Contact aided compliant mechanisms: concept and preliminaries. In *International design engineering technical conferences and computers and information in engineering conference*, volume 36533, pages 109–121, 2002.

[2] Jesse R Cannon and Larry L Howell. A compliant contact-aided revolute joint. *Mechanism and Machine Theory*, 40(11):1273–1293, 2005.

[3] Yashwanth Tummala, Aimy Wissa, Mary Frecker, and James E Hubbard. Design and optimization of a contact-aided compliant mechanism for passive bending. *Journal of Mechanisms and Robotics*, 6(3), 2014.

[4] Anzhu Gao, Hao Liu, Yun Zou, Zhidong Wang, Ming Liang, and Zulu Wang. A contact-aided asymmetric steerable catheter for atrial fibrillation ablation. *IEEE Robotics and Automation Letters*, 2(3):1525–1531, 2017.

[5] Laura Ros-Freixedes, Anzhu Gao, Ning Liu, Mali Shen, and Guang-Zhong Yang. Design optimization of a contact-aided continuum robot for endobronchial interventions based on anatomical constraints. *International journal of computer assisted radiology and surgery*, 14(7):1137–1146, 2019.

[6] Kyle W Eastwood, Arushri Swarup, Peter Francis, Alexander N Alvara, Honzer Chen, Thomas Looi, Hani E Naguib, and James M Drake. A steerable neuroendoscopic instrument using compliant contact-aided joints and monolithic articulation. *Journal of Medical Devices*, 14(2), 2020.

[7] Vipul Mehta, Mary Frecker, and George Lesieutre. Contact-aided compliant mechanisms for morphing aircraft skin. In *Modeling, Signal Processing, and Control for Smart Structures 2008*, volume 6926, page 69260C. International Society for Optics and Photonics, 2008.

[8] Rebecca Stavely and George A Lesieutre. Variable thermal conductivity, contact-aided cellular structures for spacecraft thermal control. In *54th AIAA/ASME/ASCE/AHS/ASC Structures, Structural Dynamics, and Materials Conference*, page 1588, 2013.

[9] Nilesh D Mankame and GK Ananthasuresh. Topology optimization for synthesis of contact-aided compliant mechanisms using regularized contact modeling. *Computers & structures*, 82(15-16):1267–1290, 2004.

[10] ND Mankame and GK Ananthasuresh. Synthesis of contact-aided compliant mechanisms for non-smooth path generation. *International journal for numerical methods in engineering*, 69(12):2564–2605, 2007.

[11] Vipul Mehta, Mary Frecker, and George A Lesieutre. Topology optimization of contact-aided compliant cellular mechanisms. In *Smart Materials, Adaptive Structures and Intelligent Systems*, volume 48975, pages 305–315, 2009.

[12] BVS Nagendra Reddy, Sujitkumar V Naik, and Anupam Saxena. Systematic synthesis of large displacement contact-aided monolithic compliant mechanisms. *Journal of mechanical design*, 134(1), 2012.

[13] Prabhat Kumar, Roger A Sauer, and Anupam Saxena. Synthesis of c0 path-generating contact-aided compliant mechanisms using the material mask overlay method. *Journal of Mechanical Design*, 138(6), 2016.

[14] Prabhat Kumar, Anupam Saxena, and Roger A Sauer. Computational synthesis of large deformation compliant mechanisms undergoing self and mutual contact. *Journal of Mechanical Design*, 141(1), 2019.

[15] Prabhat Kumar, Roger A Sauer, and Anupam Saxena. On topology optimization of large deformation contact-aided shape morphing compliant mechanisms. *Mechanism and Machine Theory*, 156:104135, 2021.

[16] Ole Sigmund and Kurt Maute. Topology optimization approaches. *Structural and Multidisciplinary Optimization*, 48(6):1031–1055, 2013.

[17] Yangjun Luo, Ming Li, and Zhan Kang. Topology optimization of hyperelastic structures with frictionless contact supports. *International Journal of Solids and Structures*, 81:373–382, 2016.

[18] Gil-Eon Jeong, Sung-Kie Youn, and KC Park. Topology optimization of deformable bodies with dissimilar interfaces. *Computers & Structures*, 198:1–11, 2018.

[19] Cao Niu, Weihong Zhang, and Tong Gao. Topology optimization of continuum structures for the uniformity of contact pressures. *Structural and Multidisciplinary Optimization*, 60(1):185–210, 2019.

[20] Cao Niu, Weihong Zhang, and Tong Gao. Topology optimization of elastic contact problems with friction using efficient adjoint sensitivity analysis with load increment reduction. *Computers & Structures*, 238:106296, 2020.

[21] Hansotto Kristiansen, Konstantinos Poulios, and Niels Aage. Topology optimization for compliance and contact pressure distribution in structural problems with friction. *Computer Methods in Applied Mechanics and Engineering*, 364:112915, 2020.

[22] Gore Lukas Bluhm, Ole Sigmund, and Konstantinos Poulios. Internal contact modeling for finite strain topology optimization. *Computational Mechanics*, 67(4):1099–1114, 2021.

[23] Carlos H Villanueva and Kurt Maute. Density and level set-xfem schemes for topology optimization of 3-d structures. *Computational Mechanics*, 54(1):133–150, 2014.

[24] Matthew Lawry and Kurt Maute. Level set topology optimization of problems with sliding contact interfaces. *Structural and Multidisciplinary Optimization*, 52(6):1107–1119, 2015.

[25] Matthew Lawry and Kurt Maute. Level set shape and topology optimization of finite strain bilateral contact problems. *International Journal for Numerical Methods in Engineering*, 113(8):1340–1369, 2018.

[26] Felipe Fernandez, Michael A Puso, Jerome Solberg, and Daniel A Tortorelli. Topology optimization of multiple deformable bodies in contact with large deformations. *Computer Methods in Applied Mechanics and Engineering*, 371:113288, 2020.

[27] Soheil Soghrati, Alejandro M Aragón, C Armando Duarte, and Philippe H Geubelle. An interface-enriched generalized fem for problems with discontinuous gradient fields. *International Journal for Numerical Methods in Engineering*, 89(8):991–1008, 2012.

[28] Sanne J van den Boom, Jian Zhang, Fred van Keulen, and Alejandro M Aragón. An interface-enriched generalized finite element method for level set-based topology optimization. *Structural and Multidisciplinary Optimization*, 63(1):1–20, 2021.

[29] Peter Wriggers and Tod A Laursen. *Computational contact mechanics*, volume 2. Springer, 2006.

[30] Klaus-Jürgen Bathe. The inf–sup condition and its evaluation for mixed finite element methods. *Computers & structures*, 79(2):243–252, 2001.

[31] Anita Hansbo and Peter Hansbo. A finite element method for the simulation of strong and weak discontinuities in solid mechanics. *Computer methods in applied mechanics and engineering*, 193(33-35):3523–3540, 2004.

[32] Chandrasekhar Annavarapu, Randolph R Settgast, Scott M Johnson, Pengcheng Fu, and Eric B Herbold. A weighted nitsche stabilized method for small-sliding contact on frictional surfaces. *Computer Methods in Applied Mechanics and Engineering*, 283:763–781, 2015.

[33] Rabii Mlika, Yves Renard, and Franz Chouly. An unbiased nitsche's formulation of large deformation frictional contact and self-contact. *Computer Methods in Applied Mechanics and Engineering*, 325:265–288, 2017.

[34] JT Oden. Exterior penalty methods for contact problems in elasticity. *Nonlinear finite element analysis in structural mechanics*, pages 655–665, 1981.

[35] JO Hallquist, GL Goudreau, and DJ822741 Benson. Sliding interfaces with contact-impact in large-scale lagrangian computations. *Computer methods in applied mechanics and engineering*, 51(1-3):107–137, 1985.

[36] Juan C Simo, Peter Wriggers, and Robert L Taylor. A perturbed lagrangian formulation for the finite element solution of contact problems. *Computer methods in applied mechanics and engineering*, 50(2):163–180, 1985.

[37] I Temizer, P Wriggers, and TJR Hughes. Three-dimensional mortar-based frictional contact treatment in isogeometric analysis with nurbs. *Computer Methods in Applied Mechanics and Engineering*, 209:115–128, 2012.

[38] MA Puso and JM Solberg. A dual pass mortar approach for unbiased constraints and self-contact. *Computer Methods in Applied Mechanics and Engineering*, 367:113092, 2020.

[39] Natarajan Sukumar, Nicolas Moës, Brian Moran, and Ted Belytschko. Extended finite element method for three-dimensional crack modelling. *International journal for numerical methods in engineering*, 48(11):1549–1570, 2000.

[40] John Dolbow, Nicolas Moës, and Ted Belytschko. An extended finite element method for modeling crack growth with frictional contact. *Computer methods in applied Mechanics and engineering*, 190(51-52):6825–6846, 2001.

[41] Huangcheng Fang, Dingli Zhang, Mozhen Zhou, Qian Fang, Ming Wen, and Xinyu Hu. A virtual interface-coupled extended finite element method for three-dimensional contact problems. *International Journal for Numerical Methods in Engineering*, 122(2):386–402, 2021.

[42] Basava Raju Akula, Julien Vignollet, and Vladislav A Yastrebov. Mortex method for contact along real and embedded surfaces: coupling x-fem with the mortar method. *arXiv preprint arXiv:1902.04000*, 2019.

[43] Sanne J van den Boom, Jian Zhang, Fred van Keulen, and Alejandro M Aragón. A stable interface-enriched formulation for immersed domains with strong enforcement of essential boundary conditions. *International Journal for Numerical Methods in Engineering*, 120(10):1163–1183, 2019.

[44] Thomas Buhl, Claus BW Pedersen, and Ole Sigmund. Stiffness design of geometrically nonlinear structures using topology optimization. *Structural and Multidisciplinary Optimization*, 19(2):93–104, 2000.

[45] Claus BW Pedersen, Thomas Buhl, and Ole Sigmund. Topology synthesis of large-displacement compliant mechanisms. *International Journal for numerical methods in engineering*, 50(12):2683–2705, 2001.

[46] Anders Klarbring and Niclas Strömberg. Topology optimization of hyperelastic bodies including non-zero prescribed displacements. *Structural and Multidisciplinary Optimization*, 47(1):37–48, 2013.

[47] Ricardo Doll Lahuerta, Eduardo T Simões, Eduardo MB Campello, Paulo M Pimenta, and Emilio CN Silva. Towards the stabilization of the low density elements in topology optimization with large deformation. *Computational Mechanics*, 52(4):779–797, 2013.

[48] Gil Ho Yoon and Yoon Young Kim. Element connectivity parameterization for topology optimization of geometrically nonlinear structures. *International journal of solids and structures*, 42(7):1983–2009, 2005.

[49] Fengwen Wang, Boyan Stefanov Lazarov, Ole Sigmund, and Jakob Søndergaard Jensen. Interpolation scheme for fictitious domain techniques and topology optimization of finite strain elastic problems. *Computer Methods in Applied Mechanics and Engineering*, 276:453–472, 2014.

[50] Tyler E Bruns and Daniel A Tortorelli. An element removal and reintroduction strategy for the topology optimization of structures and compliant mechanisms. *International journal for numerical methods in engineering*, 57(10):1413–1430, 2003.

[51] Reza Behrou, Reza Lotfi, Josephine Voigt Carstensen, Federico Ferrari, and James K Guest. Revisiting element removal for density-based structural topology optimization with reintroduction by heaviside projection. *Computer Methods in Applied Mechanics and Engineering*, 380:113799, 2021.

[52] Nam-Ho Kim. Introduction to nonlinear finite element analysis. pages 190–191, 2014.